U.S. DEPARTMENT OF ENERGY

PNNL-16812

Prepared for the U.S. Department of Energy
under Contract DE-AC05-76RL01830

Accounting for False Negatives in Hotspot Detection

LH Sego
JE Wilson

August 2007

Pacific Northwest
NATIONAL LABORATORY

DISCLAIMER

PACIFIC NORTHWEST NATIONAL LABORATORY
operated by
BATTELLE
for the
UNITED STATES DEPARTMENT OF ENERGY
under Contract DE-AC05-76RL01830

Printed in the United States of America

Available to DOE and DOE contractors from the
Office of Scientific and Technical Information,
P.O. Box 62, Oak Ridge, TN 37831-0062;
ph: (865) 576-8401
fax: (865) 576-5728
email: reports@adonis.osti.gov

Available to the public from the National Technical Information Service,
U.S. Department of Commerce, 5285 Port Royal Rd., Springfield, VA 22161
ph: (800) 553-6847
fax: (703) 605-6900
email: orders@ntis.fedworld.gov
online ordering: http://www.ntis.gov/ordering.htm

This document was printed on recycled paper.
(9/2003)

Accounting for false negatives in hotspot detection

Landon Sego and John Wilson

Pacific Northwest National Laboratory
August 2007

Summary

Hotspot sampling designs are used in environmental sampling to identify the location of one (or more) contiguous regions of elevated contamination. These regions are known as hotspots. The problem of how to calculate the probability of detecting an elliptical hotspot using a rectangular or triangular grid of sampling points was addressed by Singer and Wickman in 1969. This approach presumed that any sample which coincided with a hotspot would detect the hotspot without error. However, for many sampling methodologies, there is a chance that the hotspot will not be detected even though it has been sampled directly--a false negative. We present a mathematical solution and a numerical algorithm which account for false negatives when calculating the probability of detecting hotspots that are circular in shape.

1. Introduction

Hotspot sampling designs are used in environmental sampling to identify the location of one (or more) contiguous regions of elevated contamination. These regions are known as hotspots. Elevated contamination is defined as contamination that exceeds a threshold, or action level, where the action level reflects a level of risk that is unacceptable. If the sampling methodology is qualitative and only indicates the presence or absence of contamination (as opposed to a quantitative measurement), the action level is simply defined as the "presence" of contamination. The objective of a hotspot design is to determine the sample locations that will yield a high probability of detecting a hotspot of a given size and shape, if such a hotspot exists. Typically, samples are placed at the nodes of a predetermined square, rectangular, or triangular shaped grid. Hotspots are typically characterized as being circular or elliptical in shape. Hotspot design methodology is summarized by Gilbert (1987).

The problem of how to calculate the probability of detecting an elliptical hotspot using a rectangular or triangular grid of sampling points was addressed by Singer and Wickman (1969). This approach presumed that if a sample point “hit” a hotspot, the hotspot would be detected without error. However, in many situations, there is a chance that the hotspot will not be detected even though it has been sampled directly (a false negative). Likewise, it is possible that a hotspot will be "detected" even though none exist (a false positive). We assume the consequences of a false negative are more severe than those of a false positive. For this reason, we will ignore the possibility of a false positive measurement.

The Singer-Wickman algorithm can be used to calculate the probability that at least one sample point in a rectangular or triangular grid hits an elliptical hotspot of a given shape and size. In the remainder of this section, we give a heuristic explanation of the Singer-Wickman algorithm. To simplify the explanation, we will restrict ourselves to the case where the grid is a square and the hotspot is a circle. Suppose we want to be able to detect a hotspot with radius R. Select any given square (a collection of four sample points) from the grid of sample points. Now draw four circles of radius R that are centered at the four sample points of the square, indicated by the red circles in Figure 1. We assume that if there is a hotspot, it will be centered somewhere inside the square. (And if it isn't, the center of the hotspot will lie inside another equivalent square in the grid of sample points). If the center of the actual hotspot lies inside one of the red circles, then the hotspot will be detected, because it will overlap with a sample point. This is demonstrated by the green circle in Figure 1. If the center of the actual hotspot does not lie within one of the red circles, it will not be detected, as shown by the blue circle in Figure 1.

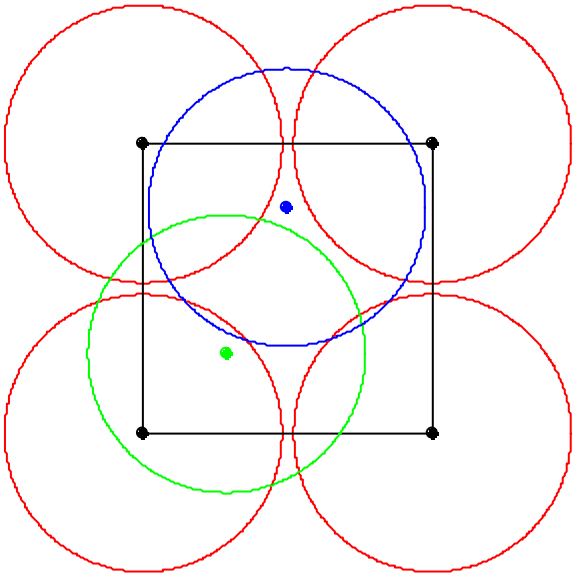

Figure 1: Illustration of the Singer-Wickman algorithm. All circles have a radius $R = 0.48$ units. The length of the side of the square, s, is 1 unit. The black points are the sample points. Hotspots with radius 0.48 units whose centers lie inside one of the red circles will be detected (e.g. green circle). Hotspots whose centers do not lie inside a red circle will not be detected (e.g. blue circle).

The strategy of the Singer-Wickman algorithm is to calculate the percentage of the area of the square that is occupied by the intersection of the square and the union of the four circles. If the circles do not overlap, the problem is trivial. However, as the radius gets larger (corresponding to a larger hotspot, or, equivalently, a smaller grid size) the circles begin to overlap, creating more complex geometric regions. In order to obtain relatively high probabilities of detecting a hotspot, the grid size must be small enough (or the hotspot large enough) for the four circles that are centered on the sample points to cover most, or all, of the square, resulting in substantial overlap among the circles. A hotspot that is centered in a region of overlap will be sampled more than once. If the false negative rate is non-zero, sampling a

hotspot more than once will increase the chance of actually detecting the hotspot. Hence, the strategy for extending the Singer-Wickman algorithm to account for false negatives is to identify the regions of double, triple, and even quadruple overlap and then calculate the area of these overlapping regions.

2. Methodology

In this section we present the methodology for calculating the probability of detecting a circular hotspot using a square, rectangular or triangular grid of sampling points while accounting for false negatives. This work builds upon the concepts of the original Singer-Wickman algorithm. The methodology relies on the following assumptions:

1. The shape of the hotspot of concern is circular.
2. The level of contamination that defines a hotspot (the action level) has been determined, which gives rise to binary outcomes. Contamination above or below the action level defines the presence or absence of a hotspot, respectively.
3. The location of the hotspot(s) is unknown, and all locations within the sampling area are equally likely to contain a hotspot.
4. Samples are taken on a square, rectangular, or triangular grid pattern.
5. Each sample is collected, handled, measured or inspected using approved methods that yield unbiased and sufficiently precise measurements.
6. A very small proportion of the surface being studied will be sampled (the sample is much smaller than the hotspot of interest).
7. Sample locations are independent of the measurement process.
8. There are no false positives (a clean area is not mistakenly identified as a hotspot)
9. The false negative rate is known and is the same for all measurements.

False negative rates are influenced by the amount of contamination that is present at the sample location. Large amounts of contamination are much more likely to be detected than trace amounts. However, for the purposes of detecting hotspots that are defined by the presence of contamination above an action level, we suggest that the false negative rate be defined as the probability that a sample measurement indicates that contamination is below the action level, when, in fact, it is at (or just above) the action level. Defining a false negative rate in this way is a conservative because it presumes that if a hotspot is present, the amount of contamination in the hotspot will be equal to the action level.

2.1 Approach for rectangular grid sampling

We begin by outlining the approach for rectangular grids (the square grid being a special case). We define below some commonly used symbols:

R = radius of circular hotspot to be detected.
s = length of the short side of the rectangle (height).
ρ = ratio of the long side to the short side of the rectangle. Hence, ρs is the length of the long side of the rectangle (width). Note that $\rho = 1$ gives a square.

$r = R/s$, the standardized radius of the hotspot.
η = false negative rate (indicated as a proportion between 0 and 1). Formally, this is the probability that the amount of contamination in a single sample is observed to be below the action level, when, in fact, it is equal to the action level.
$|\cdot|$ will denote the area function. Therefore, $|A|$ is the area of an arbitrary region A calculated using standard Euclidean geometry.
$P(r,\eta)$ is a function that gives the probability of detecting a hotspot with standardized radius r and false negative rate η.

The objective is to derive $P(r,\eta)$ for any r and η. The probability of detecting a hotspot consists of two components: 1) the probability distribution of the number of sample points that hit the hotspot, and 2) the probability that the hotspot is actually detected, given that one or more sample points have hit the hotspot.

The first component is addressed by expanding the Singer-Wickman algorithm. The likelihood of detection increases when multiple sample points hit the hotspot. The number of hits increases as the hotspot size increases (or as the grid size decreases). Since the standardized radius $r = R/s$ completely describes the proportion of the area of the rectangle that will be occupied by the four circles that are centered at the vertices of the rectangle, we can assume that $s = 1$ without loss of generality. For the present, we restrict our attention to the case where $r \leq 1$ (i.e. $R \leq s$). This prevents the circles which are centered at the sample points of adjacent rectangles from intruding upon the rectangle of interest (which occurs in Figure 3).

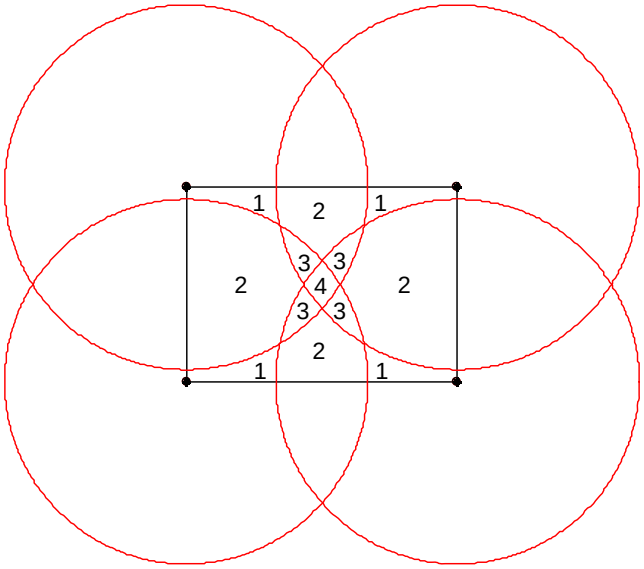

Figure 2: Regions of overlap within a rectangular sample grid of $s = 1$, $\rho = 1.4$, and $r = 0.938$. The numbers in the figure represent the number of times a hotspot would be sampled if it were centered in that region.

As we consider values of r ranging from 0 to 1, the circles centered on the sample points begin to overlap. The areas of these overlapping regions give rise to the probability distribution of the number of sample points that hit the hotspot. To describe this symbolically, let $A_1(r)$, $A_2(r)$,

$A_3(r)$, and $A_4(r)$ denote the regions inside the rectangle where a hotspot centered in that region would be sampled once, twice, thrice, or four times, respectively. These four types of regions are shown in Figure 2. Note that $A_1(r)$ is the union of the regions labeled "1", $A_2(r)$ is the union of the regions labeled "2", etc. Sometimes we refer to the regions simply as A_1, A_2, etc., even though they always depend on r.

So long as $r \le 1$, the maximum number of times a hotspot centered inside the rectangle could be sampled is four or less. Assuming that the hotspot is centered inside the rectangle, and that the distribution of the possible locations of that center point is uniform within the rectangle, the probability that a hotspot is centered in a region where it will be sampled k times is given by the area of A_k divided by the area of the rectangle: $\left|A_k\left(r\right)\right| \Big/ \left(\rho s^2\right)$. Since we assume $s = 1$, this reduces to $\left|A_k\left(r\right)\right| \Big/ \rho$. The derivations of $\left|A_k\left(r\right)\right|$, $k = 1,\ldots,4$, are given in the Appendix A.

The second component of the probability of detection is a function of the false negative rate for a single sample, η. If a single sample point hits a hotspot, the probability that a hotspot will be detected is $1 - \eta$. If two or more sampling points hit a hotspot, the probability of detecting the hotspot is equal to the probability that at least one of those sampling points detects the hotspot, or, equivalently, one minus the probability that none of those sampling points detects the hotspot, $1-\eta^2$. Consequently, the probability of detecting a hotspot that is sampled k times is $1 - \eta^k$, assuming that sample measurements are independent.

Using the law of total probability, we may combine the two components for the four levels of overlap and thereby write the probability of detecting the hotspot as a function of r and η:

$$P\left(r,\eta\right) = \frac{1}{\rho}\sum_{k=1}^{4}\left|A_k\left(r\right)\right|\left(1-\eta^k\right), \qquad 0 < r \le 1 \tag{1}$$

Depending on the value of r, $|A_k(r)|$ for $k = 2$, 3, or 4 may be zero, since the regions of multiple overlap begin to appear as r increases from zero to one.

If the false negative rate, η, is large, values of $r > 1$ may be necessary in order to achieve the desired probability of detection. While the analytical solution for $P(r,\eta)$ when $r > 1$ does exist, it becomes increasingly complicated because the circles from adjacent rectangular grids begin to encroach upon the rectangular grid of interest. This phenomenon is demonstrated with a square grid in Figure 3.

Consequently, it is convenient to approximate $P(r,\eta)$ using a numerical algorithm for values of $r > 1$. We chose to design the approximation algorithm only for $r \le 2$ because we found that for reasonable false detection rates ($\eta < 0.50$), being able to approximate $P(r,\eta)$ for values of r up to 2 units was adequate to obtain sufficiently high probabilities of detection. For example, for rectangular grids with $\rho = 1$, 2, and 3, the probability of detecting a hotspot with standardized radius of 2 units when the false negative rate is 50% is 0.9998, 0.9843, and 0.9383, respectively. However, the algorithm presented below could be constructed to approximate

$P(r,\eta)$ for virtually any finite $r > 0$. When calculating $P(r,\eta)$, we suggest using the exact solution for $0 < r \leq 1$ and the numerical approximation for $1 < r \leq 2$.

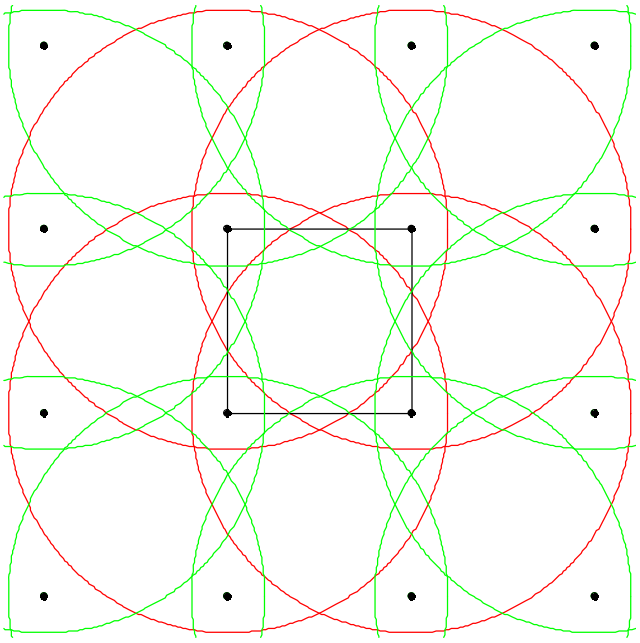

Figure 3: When $r > 1$, the circles from neighboring squares (green circles) begin to encroach upon the grid of interest (shown in black) creating many different types of overlap areas.

We describe the algorithm informally as follows. Begin with a 4×4 grid of 16 sample locations, like those shown in Figure 3. Place a dense, two dimensional array of evenly spaced "dots" inside the central rectangular grid (the grid of interest). Each dot represents the center of a possible hotspot. For each dot, count the number of the sixteen sample locations that lie within a distance r of that dot. This count represents the number of times that a hotspot of radius r centered at that dot would be "hit" by a sample location. The percentage of dots with k hits is an approximation of $|A_k(r)|$. Naturally, the approximation improves as the density of the array of dots increases. Based on comparisons of the analytical representation of $P(r,\eta)$ (given by equation (1)) and the numerical approximation of $P(r,\eta)$ for $0 < r \leq 1$, we found that arrays with around 90,000 dots provide approximations of $P(r,\eta)$ that were within 0.0027 of the true probability for an extensive number of example cases.

2.2 Approach for triangular grid sampling

The general approach for the derivation of $P(r,\eta)$ for equilateral triangular grids is essentially the same as the one described in Section 2.1 for rectangular grids. The primary difference is that the geometry of overlapping circles induced by the triangular grid results in different expressions for $|A_k(r)|$, $k = 1,\ldots,4$. We use the same notation as was used for rectangular grids, except that s will now represent the length of the side of each equilateral triangle in the grid. As before, we assume we are trying to detect a circular hotspot of radius R. Since the ratio $r = R/s$ completely describes the proportion of the area of the triangle that will be

occupied by the three circles that are centered at the vertices of the triangle, we can assume that $s = 1$ without loss of generality. The only difference in the formula for $P(r,\eta)$ for triangular grids when $0 < r \le 1$ arises in the fact that the $|A_k(r)|$ must be scaled by the area of the equilateral triangle, which is $\sqrt{3}/4$ when $s = 1$. Thus,

$$P(r,\eta) = \frac{4}{\sqrt{3}} \sum_{k=1}^{4} \left| A_k(r) \right| \left(1 - \eta^k\right), \qquad 0 < r \le 1 \tag{2}$$

Derivations of $|A_k(r)|$ for the triangular grid case are given in Appendix B.

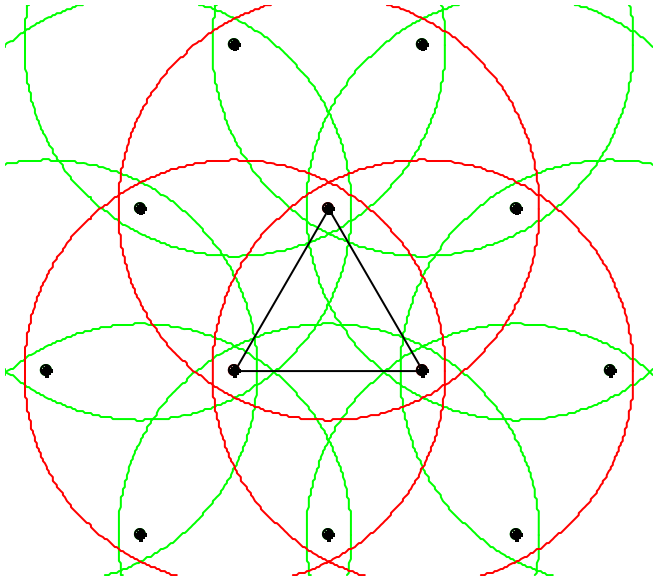

Figure 4: When $r > 1$, the encroachment of circles from neighboring triangles (green circles) increases the complexity of the overlap areas.

As with the rectangular grid case, if $r > 1$, the complexity of calculating $P(r,\eta)$ increases substantially due to the extra regions of overlap within the triangle that are created by the encroaching circles from adjacent triangles, as shown in Figure 4. For $r > 1$, a numerical approximation algorithm analogous to the one used for rectangular grids can be used. As with the rectangular grid, we designed the algorithm to approximate $P(r,\eta)$ for values of r up to 2 since $r = 2$ was sufficient to obtain high detection probabilities even when the false negative rate was high (e.g., $P(2, 0.50) = 0.9998$). To implement the algorithm, locate 12 sample points in a triangular grid as shown in Figure 4. Place a dense array of evenly spaced "dots" inside the central triangular grid (the grid of interest). Each dot represents the center of a possible hotspot. For each dot, count the number of the twelve sample locations that lie within a distance r of that dot. This count represents the number of times that a hotspot of radius r centered at that dot would be hit by a sample location. The percentage of dots with k hits is an approximation of $|A_k(r)|$. Based on comparisons of the analytical representation of $P(r,\eta)$ and the numerical approximation of $P(r,\eta)$ for $0 < r \le 1$, we found that arrays with around 45,000 dots provide approximations of $P(r,\eta)$ that were within 0.0031 of their true values. As with rectangular grids,

when calculating $P(r,\eta)$, we suggest using the exact solution for $0 < r \leq 1$ and the numerical approximation for $1 < r \leq 2$.

3. Conclusion

In this report we present a mathematical solution and a numerical algorithm which account for false negatives when calculating the probability of detecting hotspots that are circular in shape using a rectangular or triangular grid of sample points. A natural extension of this work would be to account for hotspots that are elliptical in shape.

When implementing hotspot designs, an investigator may wish to determine the size of a hotspot that can be detected for a pre-specified probability of detection and grid size. Likewise, it may be useful to determine the size of the grid that will achieve a desired detection probability for a given hotspots size. Both of these objectives could be realized by solving $P(r,\eta)$ for r analytically. However, this approach would be formidable because $\left|A_k\left(r\right)\right|$ for $k = 2,3,4$ are piecewise functions of r. A much simpler approach is to solve for r computationally using a binary search or some other numerical algorithm.

The original Singer-Wickman algorithm, as well as the mathematical solution and the numerical algorithm which account for false negatives, have all been implemented in Visual Sample Plan (VSP), a freely-available software tool for creating environmental statistical sampling designs.

References

Gilbert, R.O. (1987) *Statistical Methods for Environmental Pollution Monitoring*. John Wiley & Sons, Inc. New York, NY. pp 119--131.

Singer, D.A. and F.E. Wickman. (1969) *Probability Tables for Locating Elliptical Targets with Square, Rectangular, and Hexagonal Point Nets.* Pennsylvania State University, University Park, Pennsylvania.

Visual Sample Plan. Environmental sampling software produced by Pacific Northwest National Laboratory with support from DOE, EPA, DoD, DHS, CDC/NIOSH, TSWG, and AWE-UK. http://vsp.pnl.gov/.

Appendix A: Calculating $\left|A_k\left(r\right)\right|$ for rectangular grids when $0 < r \le 1$:

In presenting the derivations for $\left|A_k\left(r\right)\right|$, $k = 1,\ldots,4$, we begin with $\left|A_4\left(r\right)\right|$. In order for region A_4 to exist, r must be greater than $\frac{1}{2}\sqrt{1+\rho^2}$. Assuming this is the case, we can, without loss of generality, designate the lower left sample point in the square of Figure 2 as the origin. Note that A_4 is symmetric about the vertical line $x = \rho/2$ and symmetric about the horizontal line $y = ½$, and the point $(\rho/2, ½)$ lies in the center of A_4. Let A_4' denote the upper right quadrant of A_4, defined by the lines $x = \rho/2$, $y = ½$, and the arc of the lower left circle that is centered at the origin and described by the equation $x^2 + y^2 = r^2$. By translating the region A_4' such that the point $(\rho/2, ½)$ is now the origin, we have

$$\begin{aligned}\left|A_4'\left(r\right)\right| &= \int_0^{\sqrt{r^2-1/4}-\rho/2}\left(\sqrt{r^2-\left(x+\rho/2\right)^2}-1/2\right)dx \\ &= \frac{r^2}{2}\left[\arcsin\left(\frac{1}{r}\sqrt{r^2-1/4}\right)-\arcsin\left(\frac{\rho}{2r}\right)\right]+\frac{\rho}{4}\left(1-\sqrt{r^2-\frac{\rho^2}{4}}\right)-\frac{1}{4}\sqrt{r^2-1/4}\end{aligned}$$

And by the symmetry of A_4, we have:

$$\left|A_4\left(r\right)\right| = \begin{cases} 4\left|A_4'\left(r\right)\right| & \frac{1}{2}\sqrt{1+\rho^2} < r \le 1 \\ 0 & \text{otherwise}. \end{cases}$$

In order to calculate $\left|A_1\left(r\right)\right|$, $\left|A_2\left(r\right)\right|$, and $\left|A_3\left(r\right)\right|$, we define $h(r,d)$, a function that gives the area of the intersection of two circles with common radii r whose center points are d units apart. Referring to Figure A1, the strategy for determining the area of the intersection will be to calculate the area of the circle sector CAD, minus the area of triangle CAD, and then multiply the result by 2. Let d denote the distance between the centers of the circles (length of the line segment AB). Since the circles have the same radius r, note that the lengths of the line segments AE and EB are both $d/2$. And since the length of the line segment AC is r, the length of the segment CE is $\sqrt{r^2-d^2/4}$. Since CEA is a right triangle, $\theta = \arccos\left(\frac{d}{2r}\right)$. By the symmetry of triangles CEA and DEA, the area of the circle sector CAD is $\frac{2\theta}{2\pi}\pi r^2 = \theta r^2$. The area of triangle CAD is $(d/2)\sqrt{r^2-d^2/4}$.

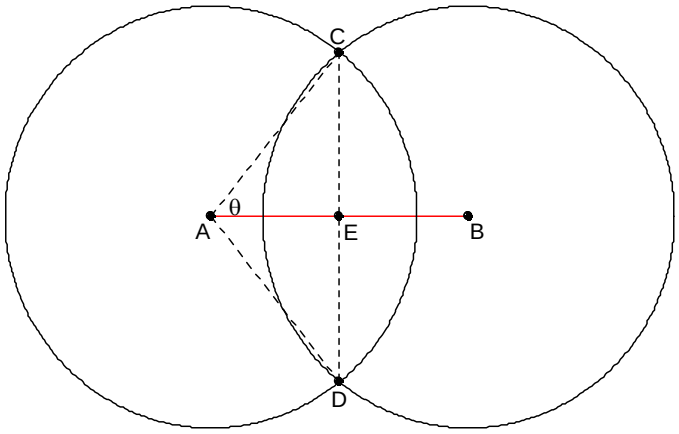

Figure A1: Diagram showing the approach for calculating the area of the intersection of two circles with common radii, *r*.

This gives

$$h\left(r,d\right)=\begin{cases} 2r^2\arccos\left(\dfrac{d}{2r}\right)-d\sqrt{r^2-\dfrac{d^2}{4}} & \text{if } r\geq\dfrac{d}{2} \\ \\ 0 & \text{otherwise .} \end{cases}$$

Referring to Figure 2, region A_3 exists when diagonal circles intersect, which occurs when $r > \frac{1}{2}\sqrt{1+\rho^2}$. Hence, $|A_3(r)|$ is given by the areas of the intersection of the diagonal circles less the twice over-counted area of $A_4(r)$:

$$\left|A_3\left(r\right)\right|=2\left(h\left(r,\sqrt{1+\rho^2}\right)-\left|A_4\left(r\right)\right|\right) \quad \text{for } 0<r\leq 1 .$$

Note that by the definition of $h(r,d)$ and $|A_4(r)|$, $|A_3(r)|$ will be 0 when $r \leq \frac{1}{2}\sqrt{1+\rho^2}$, i.e. when no region of triple overlap exists.

Figure 2 demonstrates that regions of double overlap occur when adjacent circles intersect. $|A_2(r)|$ is given by the area of the intersections of adjacent circles within the rectangle minus the over-counted regions of triple and quadruple overlap (if they are present):

$$\left|A_2\left(r\right)\right|=h\left(r,\rho\right)+h\left(r,1\right)-4h\left(r,\sqrt{1+\rho^2}\right) \quad \text{for } 0<r\leq 1 .$$

The strategy for calculating $|A_1(r)|$ is to add the areas of the four intersections of the rectangle with each of the circles and then subtract the areas of over-counted regions of double, triple, or quadruple overlap. The area of the intersection of the rectangle with a single circle is $\pi r^2/4$. Naturally, the sum of the areas of these four intersections is πr^2. By carefully subtracting the area of the over-counted regions of A_2, A_3, and A_4 (if they exist), we have:

$$\left|A_1\left(r\right)\right| = \pi r^2 - 2\left(h\left(r,\rho\right) + h\left(r,1\right) - h\left(r,\sqrt{1+\rho^2}\right) - \left|A_4\left(r\right)\right| \right) \quad \text{for } 0 < r \le 1 .$$

Appendix B: Calculating $\left|A_k\left(r\right)\right|$ for triangular grids when $0 < r \le 1$:

In presenting the derivations for $\left|A_k\left(r\right)\right|$, $k = 1,\ldots,4$, we begin with $\left|A_4\left(r\right)\right|$ for convenience. In order for region A_4 to exist, r must be greater than $\sqrt{3}/2$. Consequently, when $r > \sqrt{3}/2$, the radii of the red circles begin to extend past the sides of the triangle into adjacent triangles—and three circles from adjacent triangles begin to enter the triangle in which we are interested. This produces an area of quadruple overlap (see Figure B1). Because A_4 consists of three half-intersections of two circles whose centers are $\sqrt{3}$ units apart, we have $\left|A_4\left(r\right)\right| = \frac{3}{2} h\left(r,\sqrt{3}\right)$ for $0 \le r \le 1$ where $h\left(\cdot\right)$ is defined previously in Appendix A1. Note that the definition of $h\left(\cdot\right)$ ensures that $\left|A_4\left(r\right)\right| = 0$ when $r \le \sqrt{3}/2$.

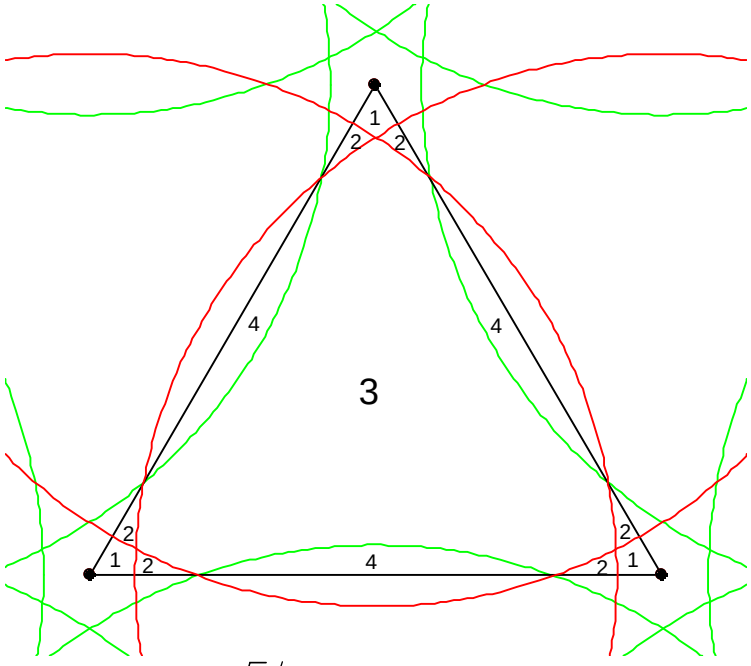

Figure B1: When r exceeds $\sqrt{3}/2$, regions of quadruple overlap begin to form.

To more easily visualize the calculation of $\left|A_3\left(r\right)\right|$, we consider A_3 when there is no quadruple overlap, as shown in figures B2 and B3. Note that region A_3 appears once $r > 1/\sqrt{3}$. To illustrate why this is so, assume without loss of generality that the lower left sample point of the triangle is at the origin. Note that the three circles will just touch one another at the point

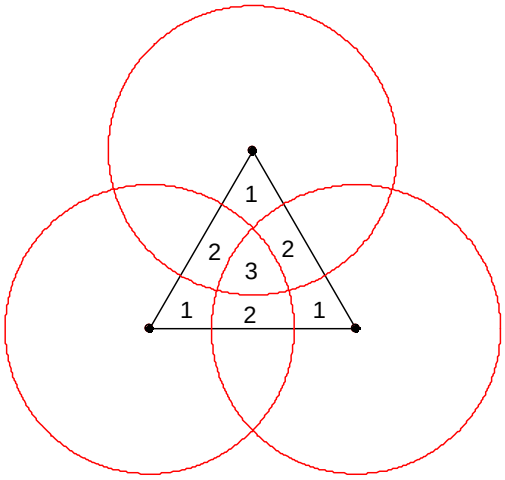

Figure B2: Numbers represent the number of times a hotspot would be sampled if it were centered in that region.

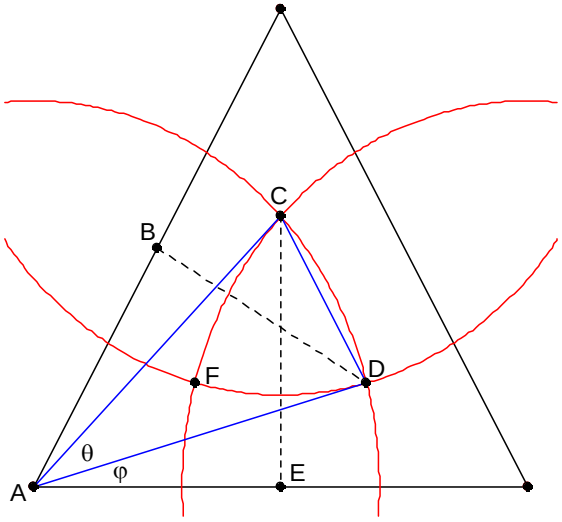

Figure B3: Diagram of the geometry used to calculate the area of the region with triple overlap, A_3.

whose Euclidean x coordinate is ½ and whose polar coordinates are $\left(r, \pi/6\right)$. Hence, the equation $1/2 = r\cos\left(\pi/6\right)$ holds at the point where the three circles touch one another, which implies that A_3 appears when $r > 1/\sqrt{3}$. We refer to Figure B3 to discuss the strategy for calculating $|A_3|$. The approach is to calculate the area of the equilateral triangle FCD and then add in the area of the three "rounded pieces" which, when added to triangle FCD, complete A_3. For example, one of

these rounded pieces is defined by the chord CD and the arc CD. The area of a single rounded piece is the difference between the areas of the circle sector ACD and the triangle ACD (shown in blue). We begin by finding angle EAC, which we define as $\xi = \varphi + \theta$. Since the segment AE has length ½ and the segment AC has length r, $\xi = \arccos\left(\frac{1}{2r}\right)$. Since triangle ABD is equivalent to a reflection of triangle ACE, angle DAB is also equal to ξ, which implies $\varphi = \pi/3 - \xi$, and, by subtraction, $\theta = 2\xi - \pi/3 = 2\arccos\left[1/(2r)\right] - \pi/3$. Hence, the area of circle sector ACD is $\theta r^2/2$. Relying on the fact that triangle ACD is isosceles, the length of segment CD is $2r\sin(\theta/2)$, and the area of triangle ACD is $\frac{r^2}{2}\sin\theta$. Using the length of segment CD, we find that the area of the equilateral triangle FCD is $\sqrt{3}\,r^2(1-\cos\theta)/2$. This gives

$$\left|A_3(r)\right| = \frac{\sqrt{3}}{2}r^2(1-\cos\theta) + 3\left(\frac{\theta r^2}{2} - \frac{r^2}{2}\sin\theta\right) = \frac{r^2}{2}\left[\sqrt{3}(1-\cos\theta) + 3(\theta - \sin\theta)\right] \quad \text{for } \frac{1}{\sqrt{3}} < r \le \frac{\sqrt{3}}{2}.$$

To generalize $\left|A_3(r)\right|$ for $0 < r \le 1$, we must constrain the value of θ at 0 when $r \le 1/\sqrt{3}$ and we must subtract twice the value of $\left|A_4(r)\right|$ when $\sqrt{3}/2 < r \le 1$ (refer to Figure B1). Therefore, let

$$\vartheta = \begin{cases} 2\arccos\left[1/(2r)\right] - \pi/3 & 1/\sqrt{3} < r \le 1 \\ 0 & \text{otherwise} \end{cases}$$

Then, $\left|A_3(r)\right| = \frac{r^2}{2}\left[\sqrt{3}(1-\cos\vartheta) + 3(\vartheta - \sin\vartheta)\right] - 2\left|A_4(r)\right|$ for $0 < r \le 1$. Note that $\left|A_3(r)\right| = 0$ when $r \le 1/\sqrt{3}$.

To explain the calculation of $\left|A_2(r)\right|$, we begin with Figure B4, which illustrates the regions of single and double overlap that are produced when $1/2 < r \le 1/\sqrt{3}$. It is clear from Figure B4 that A_2 consists of three halves of the intersection of two circles whose centers are one unit apart. Hence, $\left|A_2(r)\right| = \frac{3}{2}h(r,1)$ for $1/2 < r \le 1/\sqrt{3}$. To generalize $\left|A_2(r)\right|$ for $0 < r \le 1$, we can use Figures B1 and B2 to identify the multiples of $\left|A_3(r)\right|$ and $\left|A_4(r)\right|$ that should be

subtracted from $3h(r,1)/2$ so as not to over count the area when r exceeds $1/\sqrt{3}$. This yields $|A_2(r)| = \frac{3}{2}h(r,1) - 3|A_3(r)| - 5|A_4(r)|$ for $0 < r \le 1$. Note $|A_2(r)| = 0$ when $r < ½$.

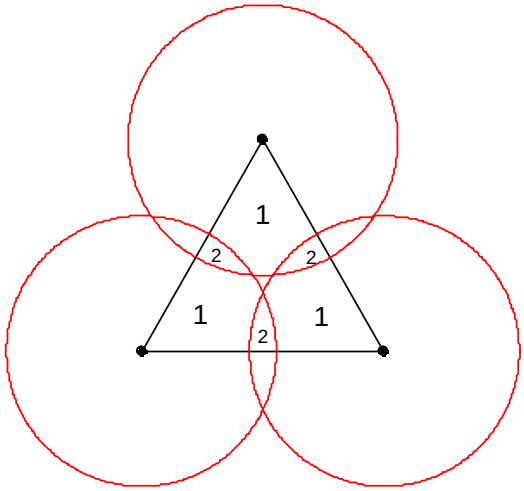

Figure B4: Coverage where adjacent circles begin to overlap, for $1/2 < r \le 1/\sqrt{3}$.

To explain the calculation of $|A_1(r)|$, we begin with Figure B5, which illustrates the regions of single overlap produced when $0 < r \le ½$. Since the triangle is equilateral, it is readily demonstrated that A_1 is a semicircle, and therefore, $|A_1(r)| = \pi r^2/2$ for $0 < r \le ½$. To generalize $|A_1(r)|$ for $0 < r \le 1$, we can use Figures B1, B2, and B4 to identify the multiples of $|A_2(r)|$, $|A_3(r)|$, and $|A_4(r)|$ that should be subtracted from $\pi r^2/2$ so as not to over count the area when r exceeds ½. This yields $|A_1(r)| = \pi r^2/2 - 2|A_2(r)| - 3|A_3(r)| - 4|A_4(r)|$ for $0 < r \le 1$.

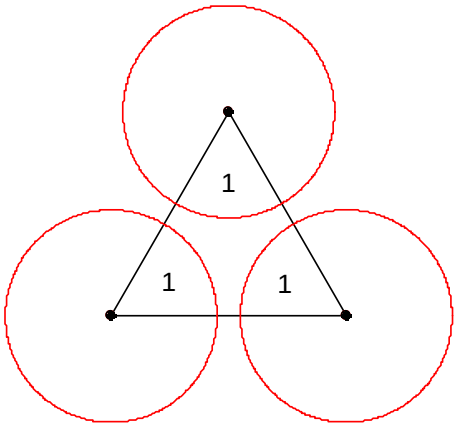

Figure B5: Coverage of the three circles when $r < ½$